JPE 18-6-25

https://doi.org/10.6113/JPE.2018.18.6.1889
ISSN(Print): 1598-2092 / ISSN(Online): 2093-4718

Harmonic Current Compensation Using Active Power Filter Based on Model Predictive Control Technology

Misbawu Adam[*,**], Yuepeng Chen[*], and Xiangtian Deng[†]

[†,*]School of Automation, Wuhan University of Technology, Wuhan, China
[**]Department of Electrical and Electronics Eng., Kumasi Technical University, Kumasi, Ghana

Abstract

Harmonic current mitigation is vital in power distribution networks owing to the inflow of nonlinear loads, distributed generation, and renewable energy sources. The active power filter (APF) is the current electrical equipment that can dynamically compensate for harmonic distortion and eliminate asymmetrical loads. The compensation performance of an APF largely depends on the control strategy applied to the voltage source inverter (VSI). Model predictive control (MPC) has been demonstrated to be one of the effective control approaches to providing fast dynamic responses. This approach covers different types of power converters due to its several advantages, such as flexible control scheme and simple inclusion of nonlinearities and constraints within the controller design. In this study, a finite control set-MPC technique is proposed for the control of VSIs. Unlike conventional control methods, the proposed technique uses a discrete time model of the shunt APF to predict the future behavior of harmonic currents and determine the cost function so as to optimize current errors through the selection of appropriate switching states. The viability of this strategy in terms of harmonic mitigation is verified in MATLAB/Simulink. Experimental results show that MPC performs well in terms of reduced total harmonic distortion and is effective in APFs.

Key words: Active power filter, Model predictive control, Total harmonic distortion, Voltage source inverters

I. INTRODUCTION

Maintaining an acceptable level of power quality has been a challenge in power systems from the early days of alternating current. The recent growing concern can be attributed to the increasing use of power electronic devices and sensitive load equipment. Large numbers of distributed nonlinear devices of small ratings, such as the power supply of most low voltage appliances (PCs and TV sets), are connected to power systems, which tend to distort the waveforms of currents and, eventually, the voltage in the grid. Although individual effects of the nonlinear devices with small ratings are insignificant, their accumulated effects can be dangerous. Large, continuously, and randomly varying nonlinear loads, such as arc furnaces, erode the quality of power supply.

The steady increase of large static power converters and power electronic devices at the transmission system level over the years and grid-connected distributed generation (DG) systems with inverters, which are known as a bridge between renewable energy sources and grids, play an essential role in many varieties of applications [1]. The high harmonic content of distorted currents and voltages can cause a heating effect, resulting in failure of power system components. This phenomenon may also distort the voltage at the point of common coupling (PCC) due to the voltage drop at their respective harmonic frequencies and equally disturb other delicate loads at the PCC [2]. The active power filter (APF) is the current electrical equipment that can dynamically compensate for harmonic distortion.

The current control of three-phase inverters in shunt active power filters (SAPF) based on voltage source inverters (VSIs) has been widely researched and executed in real industrial applications [3]. Several methods for controlling inverters,

Manuscript received Jun. 7, 2018; accepted Aug. 29, 2018
Recommended for publication by Associate Editor Hao Ma.
[†]Corresponding Author: dengxt@whut.edu.cn
Tel: +86-18071134723, Wuhan University of Technology
[*]School of Automation, Wuhan University of Technology, China
[**]Dept. of Electr. and Electron. Eng., Kumasi Technical Univ., Ghana

such as hysteresis control, proportional integral (PI) control using pulse width modulation (PWM), and model predictive control (MPC), have been investigated [4], [5]. In power electronics, hysteresis control has led to various studies on single and three-phase converters [6], [7]. Hysteresis control is also the switching technique used in APF technology [8]-[9]. However, it produces large current ripples in steady state, and its switching frequency is inconsistent. The widely used PI controllers with PWM in many types of feedback systems [10], [11] also have positive attributes, such as constant switching frequencies, closed-loop control, and small current ripples. However, obtaining the specific linear mathematical models of the plants required by PI controllers is difficult. Hence, PI controllers do not perform well under variable parameters and recent nonlinear systems. Such poor performance leads to high starting overshoot and slow response owing to unexpected disturbances [12], [13].

Since the development and improvement of digital signal processors (DSPs), MPC has been demonstrated to be one of the effective control approaches to providing fast dynamic responses to VSIs; MPC covers different types of power converters due to its several advantages, such as flexible control scheme and simple addition of nonlinearities and constraints within the controller design [14], [15]. SAPFs are extensively used to attain power quality in the grid because it can considerably reduce harmonic current and compensate for reactive power [16]. Given that the important issue in grid network is maintaining a decent power quality level to achieve security, effectiveness, and grid stability [17]-[19], MPC is an attractive option due to its characteristics and the drawbacks of classical control methods. Thus, MPC has been broadly researched and executed in power electronics and electrical drives [20], [21].

MPC has been successfully used in numerous applications, such as grid-connected DG, inverters, rectifiers, and active filters for current control [15], [20], [21], [22]. Reference [23] discussed the effective application of two types of MPC technique to a battery energy storage system (BESS) for microgrid control. Reference [24] analyzed the impact of system parameters on the control performance of MPC for frequency regulation in a typical stand-alone microgrid using a diesel engine generator, energy storage system, wind turbine, and load. Reference [25] further presented a new way to implement finite control set (FCS)-MPC for the control of four-level converters to correct the mismatch in model parameters and achieve superior performance in steady state. The energy management system of MPC in hybrid electric vehicles was presented in [26], [27]. The prediction of vehicle speed was proposed on the basis of the MPC strategy and approach to enable the energy management system of a microgrid to improve the microgrid's economic performance with consideration of various uncertainties.

For the application of this strategy, the present study takes advantage of the discrete nature of power converters and proposes FCS-MPC to regulate two-level three-phase inverters. The optimizations and predictions are considerably simplified and can be implemented in digital microprocessors because a three-phase inverter has a finite number of switching states ($2^3 = 8$). Among the classifications of MPC presented in the literature [28], FCS-MPC is the model-based control strategy with simple implementation necessary to enhance current behavior. The system is optimized by finding parameters that absolutely minimize the deviation among predicted output systems from the desired behavior.

In this study, MPC is applied to an SAPF-based two-level three-phase inverter to compensate for the harmonic currents drawn by nonlinear loads in the power system. The discrete time model of the SAPF is investigated to predict the behavior of harmonic currents and determine the cost function so as to optimize current errors through the selection of appropriate switching states. MATLAB/Simulink and experimental results are presented to attest to the effectiveness and feasibility of the proposed control strategy in APFs. The results also verify and confirm the viability of the proposed technique in harmonic mitigation.

II. System Architecture Model

A. Description of SAPF

SAPFs can be regulated to mitigate the AC line (i_{Sabc}) harmonic currents introduced by nonlinear loads. The SAPF presented in Fig. 1 comprises a VSI, whose DC side is linked to a capacitor bank (C) and whose AC side is linked to the grid through an LCL filter to inject current (i_{fabc}) that compensates for the harmonic components of nonlinear loads.

B. Reference Current Generation

In this section, the $i_p - i_q$ method [29], [30], which is typically centered on instantaneous power theory, is utilized to detect harmonic current components. These components are effectively removed from the fundamental components of the current because the source current component is distorted, as shown in Fig. 2. This figure also shows the phase-locked loop (PLL), a circuit building block particularly noted for its flexibility. PLL synchronizes the voltage control oscillator (VCO) with reference frequency through feedback to generate a stable high output frequency from a fixed low frequency signal.

VCO generates oscillating waveforms at varying frequencies. This PLL circuit block can be utilized in simple applications, such as sine and cosine signal generation ($\sin \omega t$ and $\cos \omega t$), which must be in phase with the compensating current.

The elementary working principles of the current detection circuit shown in Fig. 2 are in accordance with instantaneous power theory discussed in the literature [31]. Clark transformation

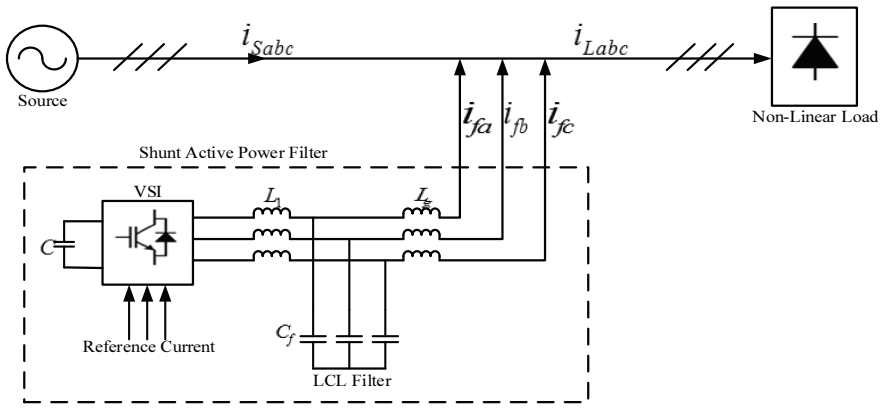

Fig. 1. Schematic of the three-wire SAPF.

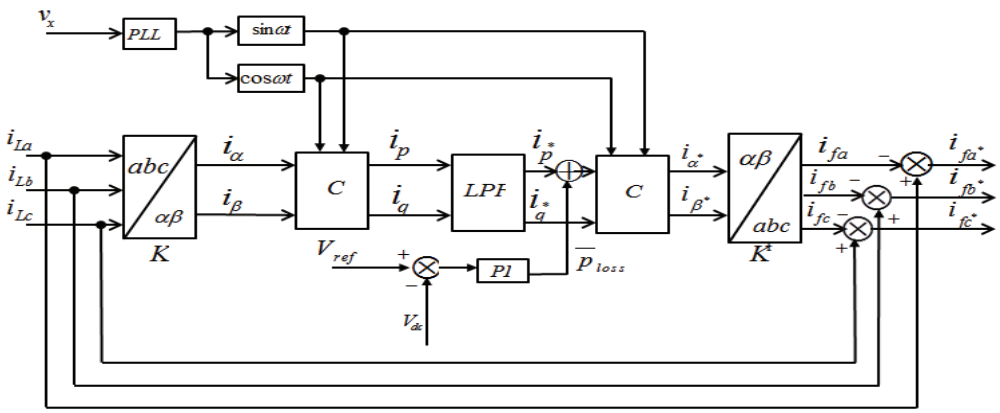

Fig. 2. General scheme of the algorithm for harmonic current detection.

matches the three-phase instantaneous line currents $i_a, i_b,$ and i_c into instantaneous currents i_α and i_β on the $\alpha\beta$ axes given by block K. The inverse Clark transformation then transforms i_α^* and i_β^* instantaneous components into the three-phase compensating current referred to as $i_{fa}, i_{fb},$ and i_{fc} given by block K'.

The fundamental reference current components $i_{fa}, i_{fb},$ and i_{fc} can be obtained as follows:

$$\begin{bmatrix} i_\alpha \\ i_\beta \end{bmatrix} = C_{3/2} \begin{bmatrix} i_a \\ i_b \\ i_c \end{bmatrix} \tag{1}$$

where,
$$C_{3/2} = \sqrt{\frac{2}{3}} \begin{bmatrix} 1 & -0.5 & -0.5 \\ 0 & \frac{\sqrt{3}}{2} & -\frac{\sqrt{3}}{2} \end{bmatrix}. \tag{2}$$

$$\begin{bmatrix} i_p \\ i_q \end{bmatrix} = C_{2/2} \begin{bmatrix} i_\alpha \\ i_\beta \end{bmatrix} \tag{3}$$

where,
$$C_{2/2} = \begin{bmatrix} \sin\omega t & -\cos\omega t \\ -\cos\omega t & -\sin\omega t \end{bmatrix}. \tag{4}$$

The instantaneous active and reactive DC components of currents i_p^* and i_q^* determined by using a low-pass filter are given as

$$\begin{bmatrix} i_\alpha^* \\ i_\beta^* \end{bmatrix} = C_{2/2} \begin{bmatrix} i_p^* \\ i_q^* \end{bmatrix}. \tag{5}$$

The fundamental current components

$$\begin{bmatrix} i_{fa} \\ i_{fb} \\ i_{fc} \end{bmatrix} = C_{3/2}' \begin{bmatrix} i_\alpha^* \\ i_\beta^* \end{bmatrix} \tag{6}$$

can be obtained; here,

$$C_{3/2}' = \sqrt{\frac{2}{3}} \begin{bmatrix} 1 & 0 \\ -0.5 & \frac{\sqrt{3}}{2} \\ -0.5 & -\frac{\sqrt{3}}{2} \end{bmatrix}. \tag{7}$$

III. Proposed FCS-MPC Strategy For Current Control

The control strategy by FCS-MPC is based on the finite numbers of switching states generated by a power converter and a model of the system that is used to predict the future behavior of the variables for each switching state. The

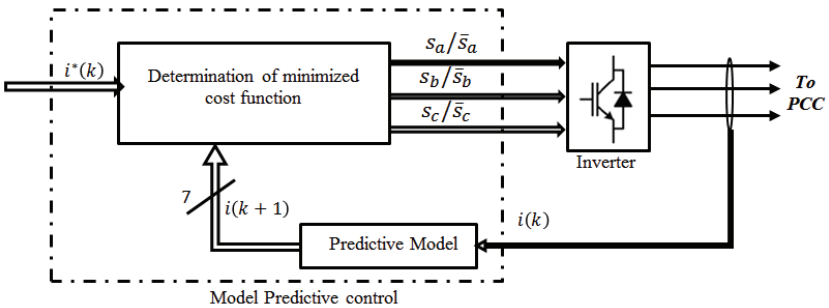

Fig. 3. Block diagram of predictive current control.

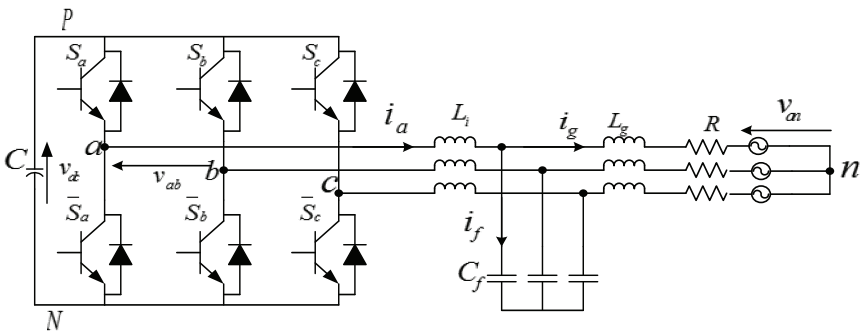

Fig. 4. Schematic of a three-phase VSI.

prediction analysis is directly derived using a discrete mathematical model and parameters of the system to consider restrictions such as sampling time, delay, and approximation [32]. All the possible control actions are compared by using a cost function to determine which of the switching control actions must be selected. This selection is usually dependent on the desired reference value, and only the switching state that reduces the cost function is selected as the best state for the subsequent sampling period. The basic idea of this control approach is summarized as follows [28]:

- The utilization of a model to predict the future behavior of variables with time.
- A cost function that represents the preferred behavior of the system.
- An optimum actuation obtained by reducing the cost function.

Fig. 3 illustrates the block diagram of the fundamental principle of FCS-MPC for power conversion.

Herein, $i^*(k)$ represents the reference currents at instant (k) for controllable variables. The actual values of the load current $i(k)$ are measured at instant (k). $i(k+1)$ is the predicted current of the states for seven possible switching states at instant $(k+1)$ with consideration of two-level three-phase inverter switching states. The reference and predicted currents are used as inputs for the predictive model to compute the values of the currents at the subsequent sampling time for each of the possible switching states of the cost function (see Eq. 8). The vector that reduces this function is applied to the next interval. Each switching state can be changed only once at every sampling instant. The main characteristic of this control strategy is the selection of a voltage vector, which reduces the cost function (g) and thus measures the error of the source current at the subsequent sampling time $(k+1)$. The cost function is expressed as a function of the reference current and predicted current errors given in the following form:

$$g = \left|i_\alpha^* - i_\alpha^p\right| + \left|i_\beta^* - i_\beta^p\right|. \tag{8}$$

where i_α^* and i_β^* are the real and imaginary parts of the future reference current, respectively; and i_α^p and i_β^p are the real and imaginary parts of the predicted source current $i(k+1)$, respectively.

A. Inverter Model

Traditionally, connectivity functions associated with each leg of an inverter play a vital role in the analysis of the inverter. Consider the schematic of a three-phase inverter in Fig. 4. Assume that the connectivity function is denoted by S_x, where $(x = (a, b, c)$. The gate signals $S_a, S_b,$ and S_c, which can take a value of 1 or 0 (on and off, respectively), are used to define the switching states such that the relationship between V_{xN} and V_{dc} is given by

$$\begin{bmatrix} V_{aN} \\ V_{bN} \\ V_{cN} \end{bmatrix} = V_{dc} \cdot \begin{bmatrix} s_a \\ s_b \\ s_c \end{bmatrix}. \tag{9}$$

The phase voltage V_{xN} can be expressed as

TABLE I
NORMALIZED VOLTAGE VECTOR IN (α,β) COORDINATES

V_x	V_0	V_1	V_2	V_3	V_4	V_5	V_6	V_7
S_a	0	0	0	0	1	1	1	1
S_b	0	0	1	1	0	0	1	1
S_c	0	1	0	1	0	1	0	1
V_α	0	$-\left(\frac{1}{3}\right)V_{dc}$	$-\left(\frac{1}{3}\right)V_{dc}$	$-\left(\frac{2}{3}\right)V_{dc}$	$\left(\frac{2}{3}\right)V_{dc}$	$\left(\frac{1}{3}\right)V_{dc}$	$\left(\frac{1}{3}\right)V_{dc}$	0
V_β	0	$-\left(\frac{\sqrt{3}}{3}\right)V_{dc}$	$\left(\frac{\sqrt{3}}{3}\right)V_{dc}$	0	0	$-\left(\frac{\sqrt{3}}{3}\right)V_{dc}$	$\left(\frac{\sqrt{3}}{3}\right)V_{dc}$	0

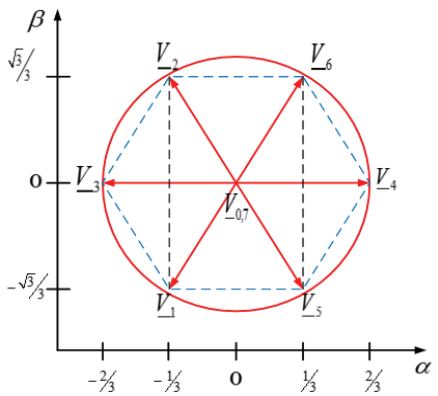

Fig. 5. Three-phase voltage in a plane.

$$\begin{bmatrix} V_{aN} \\ V_{bN} \\ V_{cN} \end{bmatrix} = \begin{bmatrix} V_{an} \\ V_{bn} \\ V_{cn} \end{bmatrix} - \begin{bmatrix} V_{nN} \\ V_{nN} \\ V_{nN} \end{bmatrix}. \tag{10}$$

Assuming that the system is balanced, the sum of the phase voltages will be equal to zero. Hence, the third equation given by

$$V_{aN} + V_{bN} + V_{cN} = 0 \tag{11}$$

is introduced to obtain a unique solution. This equation is assumed to not generate any zero sequence components.

The expression

$$V_{nN} = \frac{1}{3}\left(V_{an} + V_{bn} + V_{cn}\right) \tag{12}$$

is obtained by manipulating Eqs. (10) and (11). Substituting Eq. (12) in (10) results in the following matrix:

$$\begin{bmatrix} V_{aN} \\ V_{bN} \\ V_{cN} \end{bmatrix} = \frac{1}{3}\begin{bmatrix} 2 & -1 & -1 \\ -1 & 2 & -1 \\ -1 & -1 & 2 \end{bmatrix}\begin{bmatrix} V_{an} \\ V_{bn} \\ V_{cn} \end{bmatrix}. \tag{13}$$

System (13) is transformed into α,β coordinates. The transformation from three-phase (a,b,c) to two-phase (α,β) coordinates can be accomplished through

$$\begin{aligned} V_\alpha &= \frac{2}{3}\left(V_{aN} - \frac{1}{2}V_{bN} - \frac{1}{2}V_{cN}\right) \\ V_\beta &= \frac{2}{3}\left(+\frac{\sqrt{3}}{2}V_{bN} - \frac{\sqrt{3}}{2}V_{cN}\right) \end{aligned} \tag{14}$$

which can be separated into its real and imaginary components. The values in Table I are obtained as a function of the possible combination of switching states. With two-level three-phase inverters, seven accessible points in the plane (α,β) are obtained from eight available combinations, as illustrated in Fig. 5.

B. Load Model

From the topology of the inverter shown in Fig. 4 and according to previous literature [33], the current through C_f can be ignored while considering the impedance of C_f to be relatively larger than that of L_i and L_g. In this case, the total impedance is obtained as $L = L_i + L_g$. Hence, the total current dynamic model of the inverter is defined by a differential equation, as in reference [19], which is given by

$$V = L\frac{di}{dt} + Ri + V_g, \tag{15}$$

where $R, L, V,$ and V_g are the load resistance, load inductance, generated inverter voltage, and grid side voltage vector, respectively.

The load current (i) and the grid-side voltage (V_g) are defined as vectors given by

$$i = \frac{2}{3}\left(i_a + \alpha i_b + \alpha^2 i_c\right). \tag{16}$$

$$V_g = \frac{2}{3}\left(V_{ga} + \alpha V_{gb} + \alpha^2 V_{gc}\right). \tag{17}$$

C. Discrete Time Model

Consider the approximate Euler's forward method for functions i and k. A discrete time function of Eq. (15) for a sampling time T_s can be used to predict the future values of the current with the voltage and measured current at the k^{th} sampling period [32].

$$\frac{di}{dt} \approx \frac{i(k+1) - i(k)}{T_S}. \tag{18}$$

Substituting Eq. (18) into Eq. (15) yields the following:

$$i^p = i(k)\left(\frac{L - T_S R}{L}\right) + \left(V(k) - V_g(k)\right)\left(\frac{T_S}{L}\right) \tag{19}$$

where $i^p = i(k+1)$ is the predicted current. The discrete

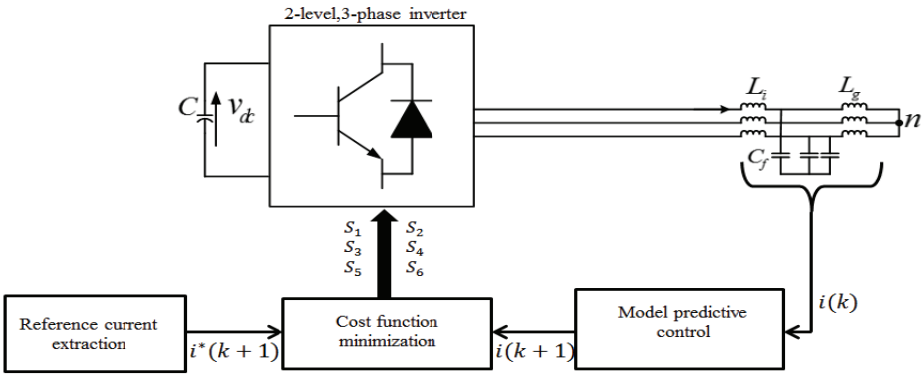

Fig. 6. Block diagram of the control connected to the two-level three-phase inverter.

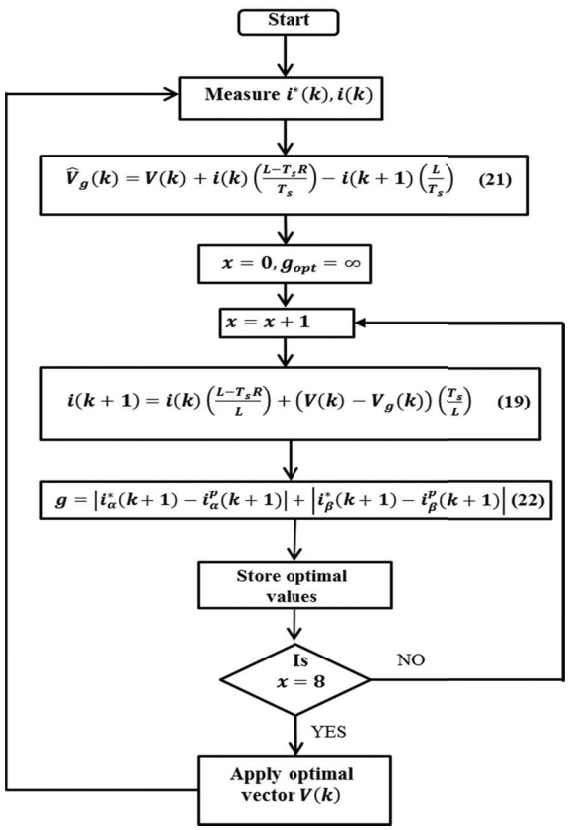

Fig. 7. Flow diagram of the MPC algorithm.

time model of the predicted currents is expressed in a state–space equation as follows:

$$\begin{bmatrix} i_\alpha^p \\ i_\beta^p \end{bmatrix} = \begin{bmatrix} \frac{L-T_sR}{L} & 0 \\ 0 & \frac{L-T_sR}{L} \end{bmatrix} \begin{bmatrix} i_\alpha(k) \\ i_\beta(k) \end{bmatrix} + \begin{bmatrix} \frac{T_s}{L} & 0 \\ 0 & \frac{T_s}{L} \end{bmatrix} \begin{bmatrix} V_\alpha(k) - V_{g\alpha}(k) \\ V_\beta(k) - V_{g\beta}(k) \end{bmatrix}. \quad (20)$$

Equation (19) is used to predict the current for every switching possibility. The cost function (g) is calculated for each of the seven possible voltage vectors generated by this inverter to estimate the future current. The voltage that reduces the cost function is chosen and applied during the subsequent sampling period.

The estimated value $\hat{V}_g(k)\ of\ V_g(k)$ can be obtained from Eq. (19) as follows:

$$\hat{V}_g(k) = V(k) + i(k)\left(\frac{L - T_sR}{T_s}\right) - i(k+1)\left(\frac{L}{T_s}\right). \quad (21)$$

D. Cost Function

A block diagram of the controller associated with the two-level three-phase inverter is illustrated in Fig. 6. As given in Eq. (22), the predicted output current is a prerequisite to the cost function computation. The algorithm calculates all the seven possible conditions that can be obtained by the state variable during the $(k+1)$ instance. The switching state in the sampling instant (k), which reduces the output current error in $(k+1)$ sampling instance, is chosen by the control strategy. The seven possible predictions achieved for $i(k+1)$ sampling period are compared with their references using the cost function (g) to choose the optimum switching state to be applied to the inverter.

$$g = \left|i_\alpha^*(k+1) - i_\alpha^p(k+1)\right| + \left|i_\beta^*(k+1) - i_\beta^p(k+1)\right|. \quad (22)$$

When the output current is equal to the reference current, $(g = 0)$. However, the objective of this cost function optimization is to obtain a (g) value near zero. The voltage vector that minimizes the cost function is chosen and applied at the next sampling instant. The key objective of the cost function is to reduce the output current error.

However, additional constraints, such as switching frequency reduction, current limitation, and spectral shaping, can be included in the cost function. The algorithm selects a switching state that produces the minimal value of the $(k+1)$ instant and is applied during the module $(k+2)$ period. Reference current value $i^*(k+1)$ is required to calculate the cost function and facilitates the selection of the optimum voltage vector.

According to previous reports [19], this reference current is unknown. Nevertheless, this reference current can be attained from the previous and present reference current values via second-order extrapolation obtained from the Lagrange

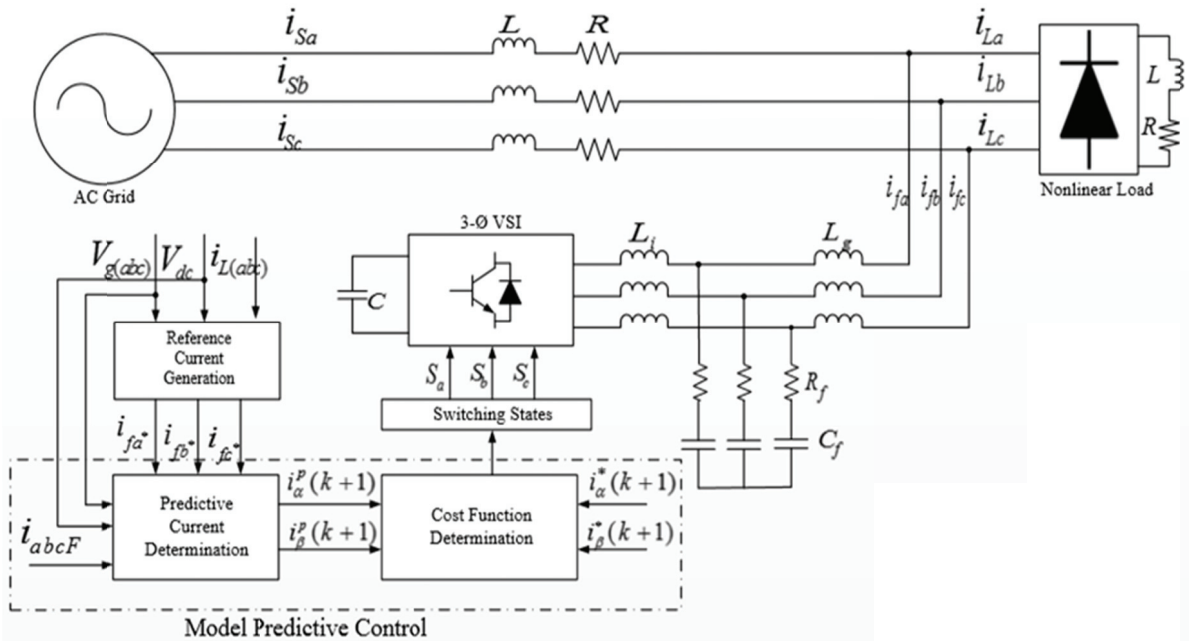

Fig. 8. Block diagram of the proposed strategy.

extrapolation formula for $n = 2$ given by Eq. (20) because it is suitable for a wide frequency range of i^*.

$$i^*(k+1) = 3i^*(k) - 3i^*(k-1) + i^*(k-2)\,. \qquad (23)$$

The reference current can also be applied to estimate $\hat{V}_g(k+1)$. However, for a sufficiently small sampling period T_s, $i^*(k+1)$ and $i^*(k)$ can be anticipated to be approximately the same. Hence, no extrapolation will be necessary. The voltage vector with the optimum cost function can be defined by the following function:

$$V_{opt} = V(g_n, \{\min\}) \quad (n = 0,1,2,3,...7) \qquad (24)$$

where g_n is the cost function for various possible switchings. The flow chart shown in Fig. 7 provides the steps to be executed to calculate the optimum cost function.

IV. Simulation and Experimental Performance Evaluation

A. Simulation Results

The performance of the proposed compensation strategy is investigated with MATLAB/Simulink to prove its feasibility in SAPF (Fig. 8). A nonlinear load that comprises a three-phase diode rectifier bridge serving an RL load is connected to a balanced three-phase voltage source.

The two-level three-phase inverter is connected to the grid through an LCL filter.

The parameters of the system are given in Table II, where V_g is the line–line voltage of the grid, F_g is the grid frequency, and F_{SW} is the switching frequency of the inverter. The sampling time is T_s, V_{dc} is the DC link voltage, and R is the nonlinear load resistance. The LCL parameters L_i and L_g correspond to the inverter- and grid-side filter inductance, respectively.

The filter capacitance and damping resistance are C_f and R_f, respectively.

Fig. 9 shows the performance between MPC and the PI controller. Two sampling times are used in the simulation analysis. In the first and final instant sampling times, $T_s = 100\,\mu s$ and $T_s = 80\,\mu s$, which are equivalent to switching frequency $F_{SW} = 10\,kHz$ and $F_{SW} = 12.5\,kHz$, respectively, are selected. The harmonic disturbances introduced by the nonlinear load current are compensated for by the generated PI-SAPF and MPC-SAPF currents. Figs. 9(a) and 9(b) show the three-phase source current and it's THDs at sampling time $T_s = 100\,\mu s$; those at sampling time $T_s = 80\,\mu s$ are presented in Figs. 9(c) and 9(d). The source current by using MPC strategy evidently has less THD compared with that when PI controller is used. The THD (up to 19th harmonic) values of the source current for the PI controller and MPC are comparable during simulation.

In Fig. 10(a), the dynamic performance of MPC is better than that of the PI controller in terms of variations in the nonlinear load resistance. The load resistance is varied from $25\,\Omega$ to $40\,\Omega$ to obtain a clear comparison of the dynamic performance of MPC and the PI controller. The comparison of the percentage THDs is also presented. With $T_s = 80\,\mu s$, the change in THD is evidently small when the nonlinear load resistance is varied using the MPC strategy; this finding is much better than that for the PI controller. Moreover, the increment in THD for the MPC strategy from $25\,\Omega$ to $40\,\Omega$ is approximately 0.4%, which is much

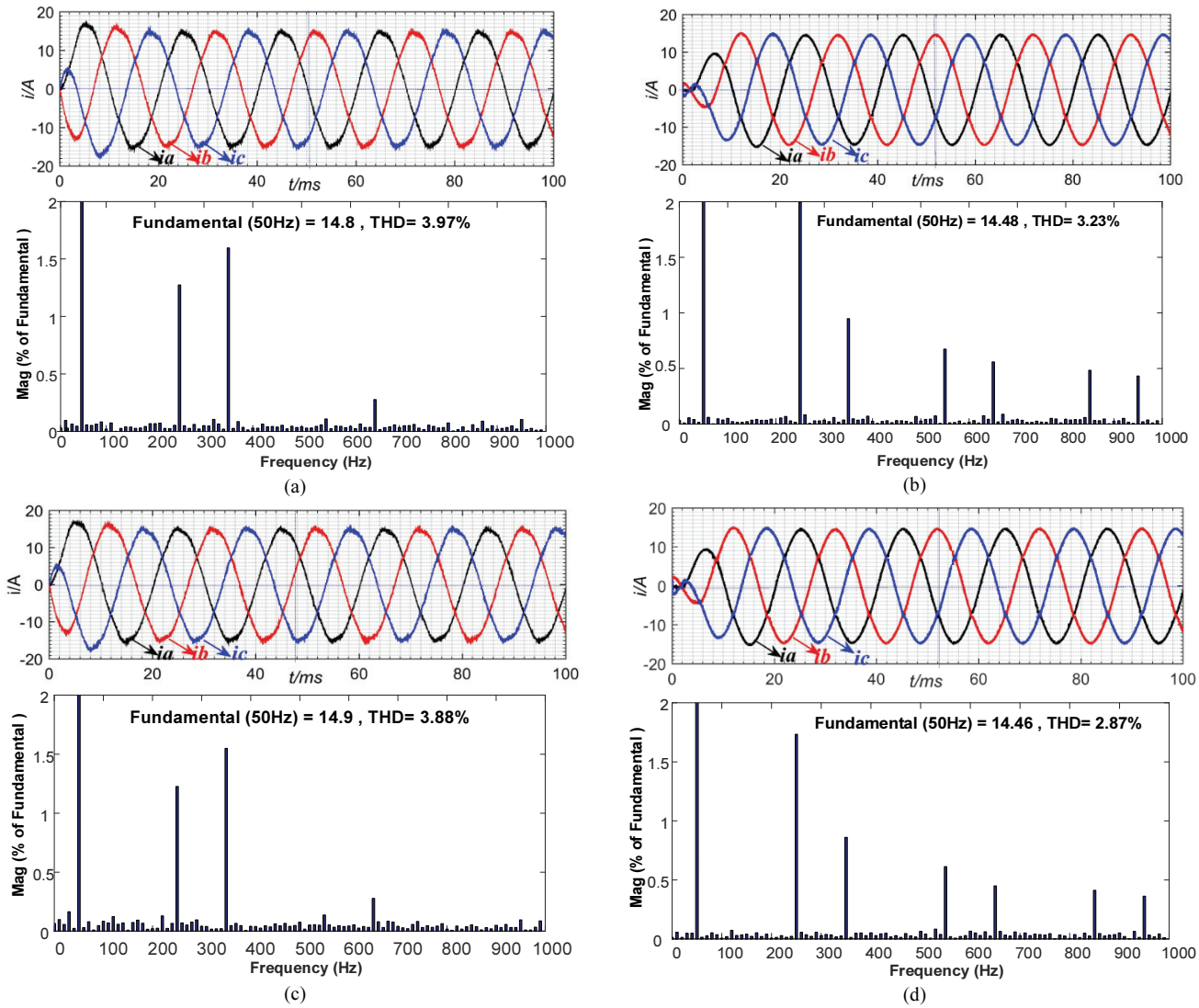

Fig. 9. Simulation performance of MPC and PI controller in terms of source current waveform and FFT analysis: (a), (c) PI controller at $F_{SW} = 10\,kHz$ and $F_{SW} = 12.5\,kHz$, respectively; (b), (d) MPC at $T_s = 100\,\mu s$ and $T_s = 80\,\mu s$, respectively.

smaller than the increment in THD for the PI controller (approximately 1.6%). This finding shows that MPC has better dynamic performance than the PI controller does. The root mean square (RMS) current value of the recorded fundamental can confirm that the MPC strategy can provide less power loss than the PI controller can.

Fig. 10(b) shows the MPC sensitivity to sampling time variations relative to its equivalent in switching frequency for the PI controller. When the switching frequency is varied from 10 kHz to 40 kHz, the THD starts to decline, but the RMS value of the fundamental current is not necessarily affected by the reduction of the THD. In particular, the THD using MPC is considerably reduced when the switching frequency is varied from 10 kHz *to* 40 kHz, whereas the THD using the PI controller slightly decreases. The MPC strategy satisfactorily performs at a sufficiently small sampling time. This finding indicates that the selection of sampling time is critical in executing the MPC strategy.

B. *Experimental Results*

An experiment is set up according to Fig. 8 and Table II to confirm the feasibility of the MPC strategy. A DSP TMS320F28335 and a field-programmable gate array (FPGA) EP4CE115F2317 serve as the control boards used to accomplish the real-time control algorithm. Infineon IGBTs are used to receive the switching signal from the DSP, and an LCL filter is used to connect the VSI to the grid. The prototype of the experimental setup shown in Fig. 11 comprises the FPGA, DSP controller, VSI, LCL filter voltage, and current measuring instruments.

Figs. 12(a)–(d) and 13(a)–(d) depict the experimental results of the MPC strategy and PI controller, respectively. Fig. 12(a) shows the nonlinear current waveform of a single phase. The nonlinear load current is clearly not sinusoidal owing to the

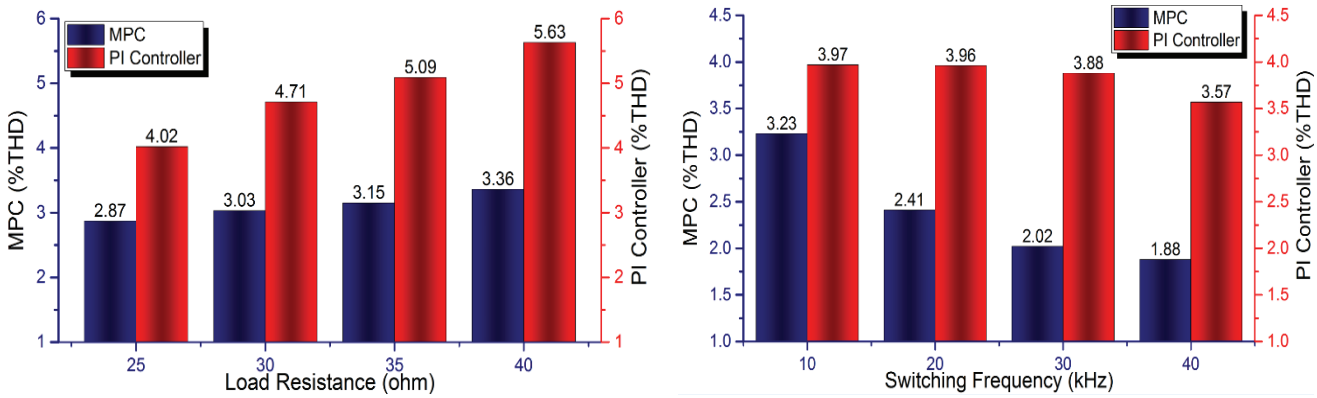

(a) (b)

Fig. 10. (a) Dynamic performance of MPC compared with that of the PI controller in terms of varied nonlinear load resistance. (b) MPC sensitivity to sampling time variations.

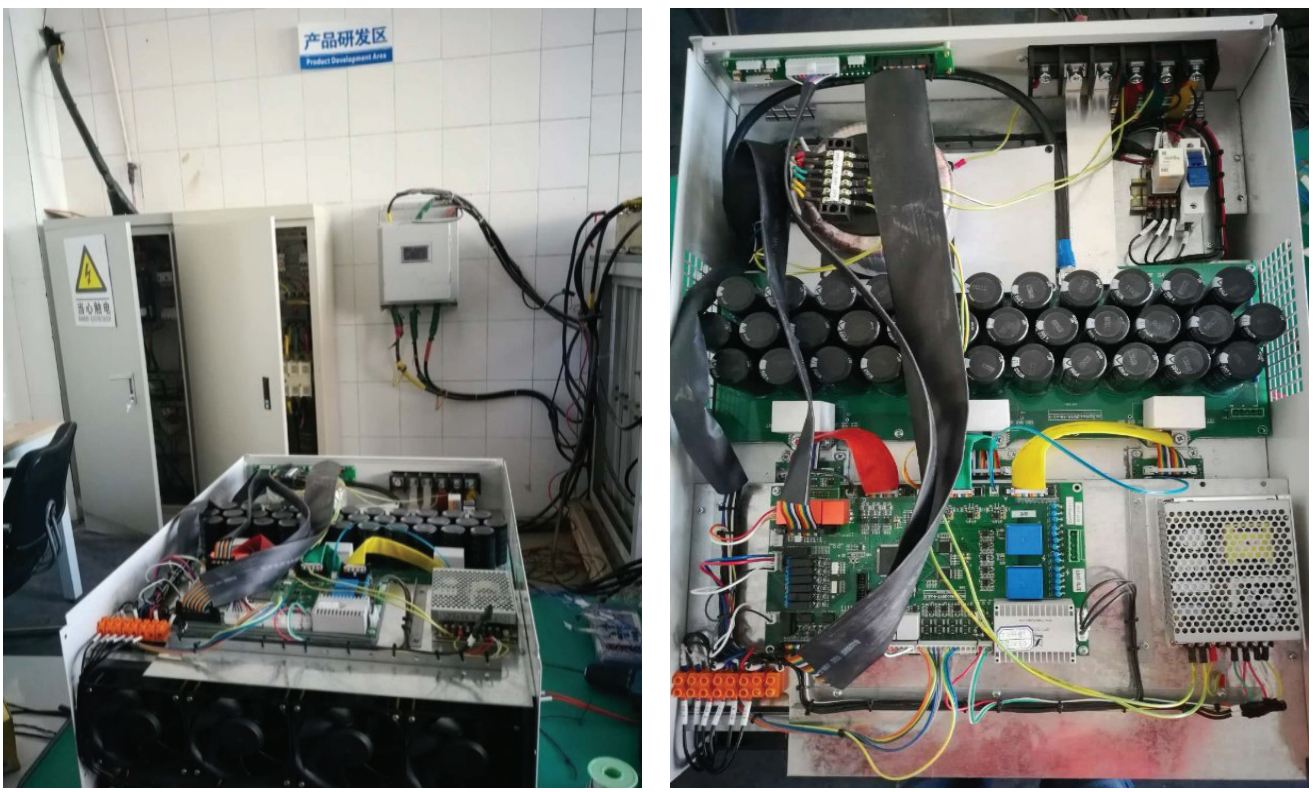

Fig. 11. Experimental setup.

presence of harmonics, which is compensated for by the APF with sampling time $T_s = 100\ \mu s$.

Fig. 12(b) depicts the compensation current, which is injected into the grid through an LCL filter at the PCC. The source current shown in Fig. 12(c) resembles a pure sine wave, which is not as smooth as that of the simulation results because sampling delay compensation exerts a considerable effect on the performance of the MPC strategy.

Given the current waveform variance in Figs. 12(c) and 13(c), the percentage THD values of the source current using the MPC and PI strategies are 3.7% and 4.3%, respectively, as shown in Figs. 12(d) and 13(d), respectively. In comparison with the PI strategy, MPC reduces the THD by 0.6%. This finding shows that the MPC strategy performs better than the PI strategy does in APFs.

The experimental results are a perfect reflection of the simulation results; however, grid voltage is sinusoidal and constant in the simulations, unlike that in a real distribution network. Thus, the current waveform in the simulation results is smoother than that in the experimental results. Nevertheless, the experimental results prove the effectiveness and feasibility of the MPC strategy in APFs.

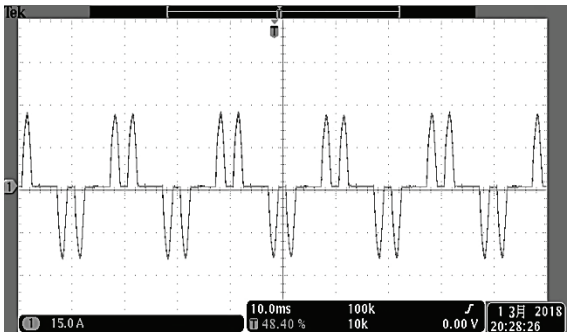

(a)

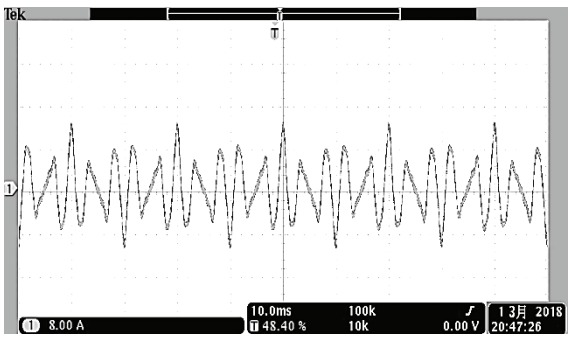

(b)

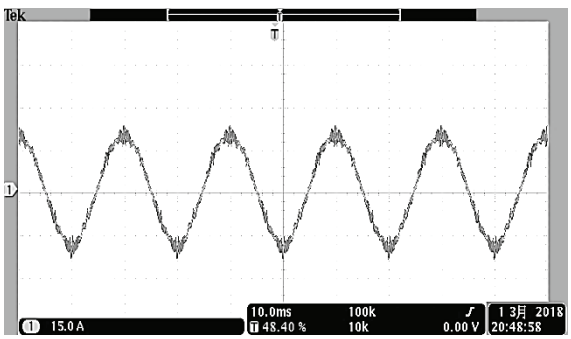

(c)

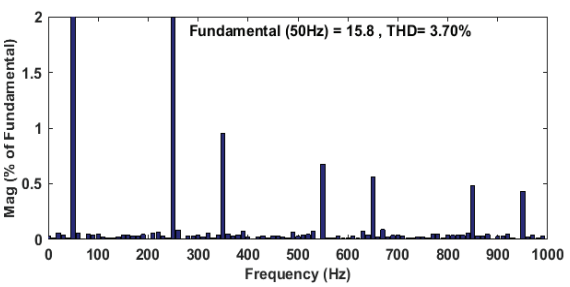

(d)

Fig. 12. Experimental results using MPC strategy at $T_s = 100$ μs. (a) Load current, (b) compensation current, and (c) source current for a single phase; (d) %THD of the source current.

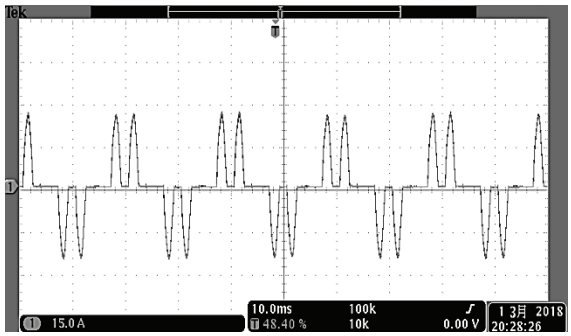

(a)

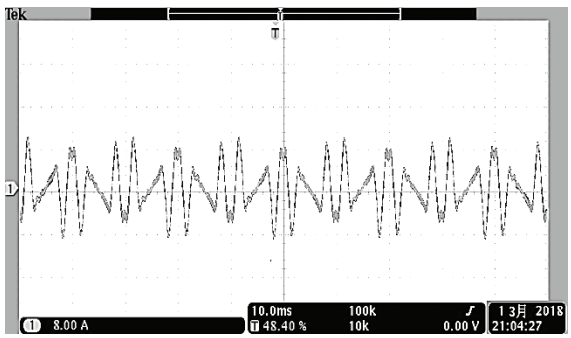

(b)

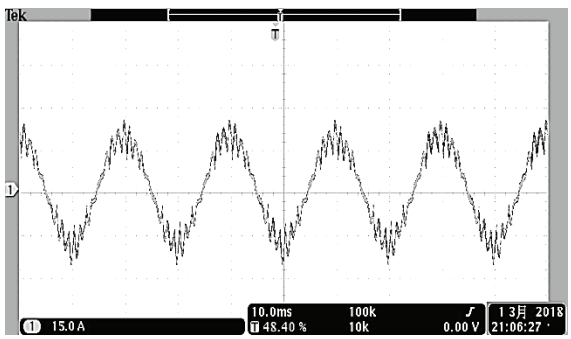

(c)

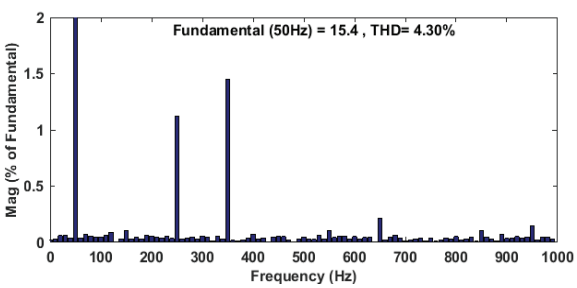

(d)

Fig. 13. Experimental results using PI control at $F_{SW} = 10\ kHz$. (a) Load current, (b) compensation current, and (c) Source current for a single phase; (d) %THD of the source current.

V. Conclusions

The determination of control strategies for APFs is among the most important issues in reducing harmonic currents to enhance the power quality of grids. This paper presents an FCS-MPC strategy that is based on SAPF to compensate for the harmonic currents caused by nonlinear loads. The proposed FCS-MPC strategy tracks harmonic currents at a rapid rate and maintains excellent control at low frequencies. The FCS-MPC strategy also provides a fast dynamic response to SAPF-based VSIs and achieves considerable system reliability at a small THD value. As indicated by the simulation results,

performance in terms of switching ripples and THD is enhanced considerably with the proposed strategy. The comparative study of the two strategies adopted in this work shows that the MPC strategy can achieve a reduced current ripple and lower THD in the source current in comparison with classical control methods. The harmonic spectrum results show the effectiveness of the proposed control strategy. Hence, the FCS-MPC approach is a viable and effective control method that compensates for harmonic currents in SAPFs.

ACKNOWLEDGMENT

The authors would like to thank Dr. Ibrahim Amin Saana, Zhenfeng Xiao, and the anonymous reviewers for their feedback and suggestions. This work was supported by the Natural Science Foundation of China (NSFC) under Grant No. 61374151, Hubei Natural Science Foundation (2018CFB205), and State Grid Hunan Electrical Power Company Science and Technology Project (5216A217000D).

REFERENCES

[1] J. He, Y. W. Li, F. Blaabjerg, and X. Wang, "Active harmonic filtering using current-controlled grid-connected DG units with closed-loop power control," *IEEE Trans. Power Electron.*, Vol. 29, No. 4, pp. 29, 642-653, Feb. 2014.

[2] G. S. Mahesh, H. M. R. Kumar, and R. P. Mandi, "Characterization of power system attributes for nonlinear loads through sub-space signal methods," *in Proc. IEEE International Conference on Power Electronics, Drives and Energy Systems (PEDES)*, pp. 1-5, 2016.

[3] Y. Zhang, W. Xie, Z. Li, and Y. Zhang, "Model predictive control of a PWM rectifier with duty cycle optimization," *IEEE Trans. Power Electron.*, Vol. 28, No. 11, pp. 5343-5351, Nov. 2013.

[4] M. Eric, *Power Electronic Converters (PWM Strategies and Current Control Techniques)*, John Wiley, 2011.

[5] N.-Y. Dai, M.-C. Wong, N. Fan, and H. Ying-Duo, "A FPGA-based generalized pulse width modulator for three-leg center-split and four-leg voltage source inverters," *IEEE Trans. Power Electron.*, Vol. 23, No. 3, pp. 1472-1484, May 2008.

[6] A. Mertens, "Performance analysis of three phase inverters controlled by synchronous delta modulation system," *IEEE Trans. Ind. Appl.*, Vol. 30, No. 4, pp. 1016-1027, Aug. 1994.

[7] R. Uhrin and F. Profumo, "Analysis of spectral performance of resonant DC link inverter controlled by delta-sigma modulation," in *Proc. EPE'95*, pp. 760-764, 1995.

[8] Y. K. Chauhan, S. K. Jain, and B. Singh, "A prospective on voltage regulation of self-excited induction generators for industry application," *IEEE Tran. Ind. Appl.*, Vol. 46, No. 2, pp. 720-730, Apr. 2010.

[9] M. Suresh, A. K. Panda, S. S. Patnaik, and Y. Suresh, "Comparison of two compensation control strategies for SHAF in 3ph 4wire system by using PI controller," in *Proc. IICPE,* pp. 1-7, 2012.

[10] N. Mohan, T.M Underland, and W. P. Robbins, *Power Electronics,* Wiley, 1995.

[11] S. Sinthusonthishat and N. Chuladaycha, "A simplified modulation strategy for three-leg voltage source inverter fed unsymmetrical two winding induction motor," *J. Elect. Eng. Technol.,* Vol. 8, pp. 1334-1337, 2013.

[12] X. Wei, "Study on digital PI control of current loop in active power filter," in *Proc. International Conference of Electrical Control Engineering*. pp. 4287-4290, 2010.

[13] S. A. Bhatti, S. A. Malik, and A. Daraz, "Comparison of P-I and I-P controller by using Ziegler-Nichols tuning method for speed control of DC motors," in *Proc. International Conference on Intelligent System Engineering (ISICE)*, pp. 326-329, 2016.

[14] T. H. Nguyen and K. H, Kim, "Finite control set- model predictive control with modulation to mitigate harmonic component in output current for a grid-connected inverter under distorted grid conditions," *Energies,* Vol. 10 pp. 1-25, Jul. 2017.

[15] R. P. Aguilera, P. Lezana, and D. E. Quevedo, "Finite-Control-Set model predictive control with improved steady-state performance," *IEEE Trans. Ind. Informat.,* Vol. 9, No. 2, pp. 658-667, May 2013.

[16] R.C. Dugan, M.F. McGranaghan, and H. W. Beaty, *Electrical Power Systems Quality*, McGraw-Hill, 1996.

[17] J. He, Y. W. Li, and M. S. Munir, "A flexible harmonic control approach through voltage-controlled DG-grid interfacing converters," *IEEE Trans. Ind. Electron.*, Vol. 59, No.1, pp. 444-455, Jan. 2012.

[18] P. Salmeron and S.P. Litran, "Improvement of the electric power quality using series active and shunt passive filters," *IEEE Trans. Power Del*. Vol. 25, No. 2, pp. 1058-1067, Apr. 2010.

[19] J. Rodriguez, J. Pontt, C. A. Silva, P. Correa, P. Lezana, P. Cortes, and U. Ammann, "Predictive current control of a voltage source inverter," *IEEE Trans. Ind. Electron*. Vol. 54, No. 1, pp. 495-503, Feb. 2007.

[20] G. Du, Z. Liu, F. Du, and J. Li, "Performance improvement of model predictive control using control error compensation for power electronic converters based on the Lyapunov function," *J. Power Electron.*, Vol. 17, No. 4, pp. 983-990, Jul. 2017.

[21] B. Feng and H. Lin, "Finite control set model predictive control of AC/DC matrix converter for grid-connection battery energy storage application," *J. Power Electron.*, Vol.15, No. 4, pp. 1006-1017, Jul. 2015.

[22] M. Rivera, L. Tarisciotti, P. Wheeler, and P. Zanchetta, "Predictive control of an indirect matrix converter operating at fixed switching frequency and without weighting factors," in *Proc. 24th International. Symposium of the IEEE Industrial Electronics,* pp. 1027-1033, 2015.

[23] T. N. Nguyen, H.-J. Yoo, and H.-M. Kim, "Application of model predictive control to BESS for microgrid control," *Energies,* Vol. 8, No. 8. pp. 8798-8813, Aug. 2015.

[24] T. N. Nguyen, H.-J. Yoo, and H.-M. Kim, "Analyzing the impact of system parameters on MPC-based frequency control for stand-alone microgrid," *Energies,* Vol. 10, No. 4, pp. 1-17, Mar. 2017.

[25] M. Norambuena, P. Lezana, and J. Rodriguez, "Improved steady sate behavior of finite control set model predictive control applied to a flying capacitor converter," *IEEE*

Energy Conversion Congress and Exposition, pp. 1-5, 2016.
[26] Z. Ji, H. Xueliang, X. Changfu, and S. Houtao. "Accelerated model predictive control for electric vehicle integrated microgrid energy management: A hybrid robust and stochastic approach," *Energies*, Vol. 9, No. 11, pp. 1-18, Nov. 2016.
[27] J. Lian, L. Shuang, L. Linhui, Z. Yafu, Y. Fan, and Y. Lushan, "A mixed logical dynamical-model predictive control (MLD-MPC) energy management control strategy for plug-in hybrid electric vehicles (PHEVs)," *Energies,* Vol. 10, No. 1, pp. 1-18, Jan. 2017.
[28] J. Rodriguez and P. Cortes, *Predictive Control of Power Converters and Electric Drives*, Wiley-IEEE, 2012.
[29] C. Yi, L. Tianfa, D. Changwen, Z. Hongwei, and X. Jiaxiang, "Study on harmonic current detection method for single-phase PV inverter," in *Proc. IEEE China International Conference on Electricity distribution*, pp. 1621-1624, 2014.
[30] H. Huang, H. Xue, X. Liu, and H. Wang, "The study of active power filters using a universal harmonic detection method," in *Proc. IEEE ECCE Asia Downunder*, pp. 591-595, 2013.
[31] V. M. Quang, H. Wei, W. Dazhi, and W. Xuming "A new type of PWM rectifier with function of harmonic suppression and reactive power compensation," in *Proc. IEEE 25th Chinese Control and Decision Conference*, pp. 3013-3017, 2013.
[32] Y. Zhang and Y. Peng, "Model Predictive Current Control with Optimal Duty Cycle for Three-Phase Grid-Connected AC/DC Converters," *in proc. IEEE International Power Electronics and Application Conference*, pp. 837-842, 2014.
[33] S.-Y. Park, J.-S. Lai, and W-C. Lee, "An easy, simple, and flexible control scheme for a three-phase grid-tie inverter system," in *proc. IEEE Energy Conversion Congress and Exposition*, pp. 599-603, 2010.

Misbawu Adam was born in Kumasi, Ghana. He received his B.S. degree in Electrical and Electronics Engineering from Kwame Nkrumah University of Science and Technology, Kumasi, Ghana, in 2011; and his M.S. degree in Power Electronics and Power Drives from Wuhan University of Technology, Wuhan, China, in 2015. He is currently working toward his Ph.D. degree in Traffic Information Engineering and Control in the field of Power Electronics in the same institution. His research area is power quality, specifically active power filters.

Yuepeng Chen received his M.S. degree in Applied Mathematics from Northeastern University, Shenyang, China, in 2001. He received his Ph.D. degree in Control Theory and Control Engineering from Northeastern University Shenyang, China, in 2005. He finished his two-year postdoctoral work in Mechatronics Engineering, Wuhan University of Technology, Wuhan, China. From 2007 to 2008, he was a visiting Professor in Monash University, Australia. He is currently a Professor in the School of Automation, Wuhan University of Technology, Wuhan, China. His current research interests include robust control, fault diagnosis, fault tolerant control, and power quality.

Xiangtian Deng received his Ph.D. degree in Electrical Engineering from Wuhan University, Wuhan, China, in 2015. He is currently an Assistant Professor in the Department of Electrical Engineering, School of Automation, Wuhan University of Technology, China. His current research interests include power quality and protection of complex power grids.